

# Fabrication and characterization of Mach–Zehnder interferometer based on a hollow optical fiber filled with radial-aligned liquid crystal

Bo-Yan Ho<sup>1</sup>, Fenglin Peng<sup>2</sup>, Shin-Tson Wu<sup>2</sup> and Shug-June Hwang<sup>1,2</sup>

<sup>1</sup> Department of Electro-Optical Engineering, National United University, Maio-Li, 360, Taiwan

<sup>2</sup> College of Optics and Photonics, University of Central Florida, Orlando, FL 32816, USA

E-mail: [june@nuu.edu.tw](mailto:june@nuu.edu.tw)

Received 16 February 2016, revised 10 May 2016

Accepted for publication 20 May 2016

Published 15 June 2016



## Abstract

We demonstrate a high sensitivity all-fiber Mach–Zehnder interferometer (MZI) based on radial-aligned liquid crystal (LC) in a hollow optical fiber (HOF). The transmission spectrum of the liquid crystal-filled fiber MZI (LCF-MZI) was measured at different temperatures, and the thermal-induced wavelength shift of the interference spectrum probed. The experimental results indicate that the LC alignment and refractive indices inside the hollow capillary are significantly influenced by the temperature, which in turn changes the optical properties of LCF-MZI. Our experimental data on notch wavelength shift agree well with the measured refractive index temperature gradient.

Keywords: Mach–Zehnder interferometer, hollow optical fiber, liquid crystal, liquid crystal device

(Some figures may appear in colour only in the online journal)

## 1. Introduction

Hollow optic fiber (HOF) has attracted considerable interest because it holds great potential applications for telecommunication, mode converter, fiber laser, nonlinear optics, and high sensitivity sensor [1–9]. To achieve tunable and multifunctional fiber devices based on HOF, liquid crystal (LC) material is often infiltrated into the cylindrical capillary because its refractive index and molecular alignment can be modulated by an external stimulus, such as temperature, electric field, and stress. Compared to a conventional optical fiber, the LC-filled fiber (LCF) offers a greater controllability on the optical properties and creates new possibilities in optical communication and sensing technology. Accordingly, LCF creates a pronounced opportunity to make new generation of advanced photonic devices, such as fiber grating, tunable attenuators and filters, polarization controllers, and sensor, etc [10–16].

In this work, we experimentally demonstrate a new alternative to previous types of all fiber Mach–Zehnder interferometer (MZI) devices [17, 18] by sandwiching a LCF with radial-aligned LC molecules between the two single mode fibers. The optical properties and tuning range of the proposed MZI are mainly determined by the LC refractive index and alignment configuration inside the air core of HOF. Here we achieved radical LC alignment in the cylindrical tubes by coating a homeotropic alignment layer on the cavity-wall surface. Together with vertical anchoring, elastic forces, and injection capillary force, we have successfully obtained radical LC alignment configuration in HOF. The realized alignment structure and temperature-induced LC reorientation were studied by means of polarizing microscopy. And the interference properties of the proposed LCF-MZI are measured by the optical spectrum analyzer, and its thermal-optic properties are experimentally studied and discussed. Due to the distinctive features of high temperature dependent refractive index

and profound temperature-induced LC reorientation, the transmission spectrum of such an interferometer fiber can be thermally tuned by changing the temperature. As a result, the proposed interferometer can achieve a large tuning range for peak wavelength by thermal modulation. The key advantages of the proposed LCF-MZI are high sensitivity, compact, simplicity, and cost effective.

## 2. Background theory and experimental

We first developed a simple method to fabricate an all-fiber MZI based on LC-infiltrated HOF with planar alignment [19]. The structure of the proposed device is constructed by splicing a LC-infiltrated HOF with length  $L$  between two standard single-mode fibers (SMFs) as shown in figure 1. When the fundamental mode propagating through the lead-in SMF core enters the HOF, it is divided into two main parts by the first abrupt tapered section symbolized by  $I_{co}$  and  $I_{clad}$ , respectively. The core mode  $I_{co}$  directly passes through the air core and LC-infiltrated section of HOF, and the cladding mode  $I_{clad}$  propagates along the core-cladding boundary. The core mode and cladding mode propagate along the HOF with different optical path length and then are recombined as they pass through the second abrupt tapering segment. Therefore the interference occurs at the lead-out SMF and the interference signal is expressed as:

$$I = I_{co} + I_{clad} + 2\sqrt{I_{co} I_{clad}} \cos \left[ \frac{2\pi (n_{eff}^{co} - n_{eff}^{clad}) L}{\lambda} \right]. \quad (1)$$

where  $I_{co}$  and  $I_{clad}$  are the intensity of light guiding in the fiber core and cladding, respectively;  $L$  stands for the interferometer length including the air cavity and LC-filled section of the HOF,  $n_{eff}^{co}$  and  $n_{eff}^{clad}$  are the effective refractive indices of the core and cladding, respectively, and  $\lambda$  is the wavelength. The optical path difference accumulated over the HOF-based MZI is  $(n_{eff}^{co} - n_{eff}^{clad}) L = \delta n_{eff} L = \delta n_{eff}^{LC} L_{LC} + \delta n_{eff}^{air} (L - L_{LC})$ , where  $\delta n_{eff}^{LC}$  and  $\delta n_{eff}^{air}$  represent the difference of the effective refractive indices between the core mode and the cladding mode for the LC section and air cavity, respectively. Due to the interference effect between different pairs of modes, the transmitted intensity reaches its minimum value, called transmission notch, when the phase difference between two modes is equal to an odd multiple of  $\pi$  (i.e.  $(2m + 1)\pi$ ,  $m$  is an integer). Thus, the notch wavelength  $\lambda_m$  of the interference beam reaching its peak can be expressed as  $\lambda_m = 2\delta n_{eff} L / (2m + 1)$ , here  $m$  is the interference order. So the notch wavelength  $\lambda_m$  of the interference with specific order in the transmission spectrum can be tuned by changing  $\delta n_{eff}$  or  $L$  through thermal effect or electric field.

To realize the proposed device, a hollow optical fiber (Polymicro, Inc.) with the nominal inner and outer diameters of  $5 \mu\text{m}$  and  $125 \mu\text{m}$  were used. And the nematic liquid crystal (NLC) used here was LCT-10-1140 (Merck) with ordinary refractive index  $n_o = 1.480$  and extraordinary refractive index  $n_e = 1.581$  at  $\lambda = 630 \text{ nm}$  and  $T = 25 \text{ }^\circ\text{C}$ , respectively. Because HOF is a capillary, the conventional alignment treatment for LC display is unsuitable to produce homogeneous

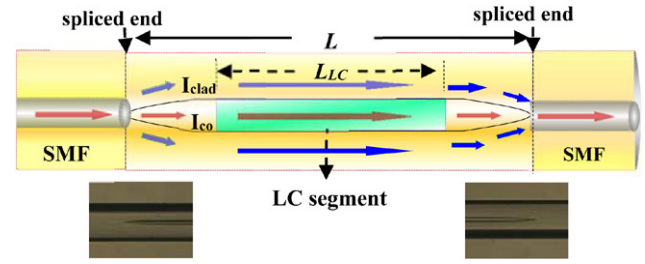


**Figure 1.** Schematic diagram of the LCF-MZI fiber, in which the tapering structure was constructed at both of the spliced ends by arc-fusing, in which  $I_{co}$  and  $I_{clad}$  are the intensity of light guiding in the fiber core and cladding, respectively.

or homeotropic surface alignment on the HOF wall surface. To obtain axial alignment inside HOF and make the LCs aligned stably under various external disturbance, here we demonstrated a simple method to form LC vertical alignment layer on the interior surface of HOF by soaking the capillarity into the vertical polyimide (PI) solution. First, we infiltrated the polyimide solution AL60101 (JSR) as a homeotropic orienting material into the hollow fiber by capillary forces, and then extracted it out of HOF after about one hour. This sufficiently long time is required to make an alignment layer well deposited on the inner capillary wall. Then the PI-coated HOF was pre-baked at  $100 \text{ }^\circ\text{C}$  on a hot plate and baked in a temperature oven for one hour. Next, we injected the LC material into the HOF by capillary flow and the infiltration length was controlled at  $\sim 4.0 \text{ mm}$ . After completing the infiltration of LC sector, the two end faces of the LC-filled HOF were spliced to two SMFs by using a fusion splicer (FITELE S175). We optimized the splicing conditions of arc power level and fusion time as 64 and 4.5 s to form abrupt tapering structure at the two spliced joints during the splicing. As mentioned above, the tapering sections function as a beam splitter and combiner, and then generate the interference signal at the output SMF. In this work, the total length of the air core at the front and rear ends of HOF is fixed at about 6.6 mm.

The interference spectral characteristics of the proposed MZIs were studied under different temperatures. Figure 2 depicts the experimental setup for measuring the transmission spectra of the LCF-MZI. One end of the LCF-MZI was connected to a broadband light source (BLSS101B-028002A; GIP Tech. Corp.), and the other end was connected to an optical spectrum analyzer (Anritsu MS9740A) with the wavelength band from 1250 nm to 1600 nm to record the transmission spectrum. A temperature controller was applied to heat the MZI fiber and the transmitted light spectrum through this interferometer was measured under different temperatures from  $30 \text{ }^\circ\text{C}$  to  $130 \text{ }^\circ\text{C}$ . To monitor the real temperature of the LCF-MZI controlled by the thermoelectric-cooling system, a thermal sensor was also applied during the spectrum measurement.

## 3. Results and discussion

To identify the LC alignment and the quality of LC-infiltration in the HOF, we observed the LCF using a polarizing optical microscope (POM) between crossed polarizers. Figure 3

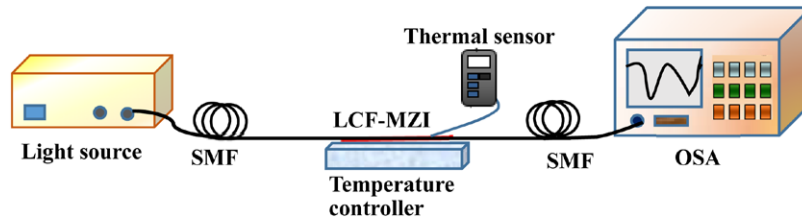


Figure 2. Experimental setup for measuring the transmission spectrum of radical-aligned LCF-MZI.

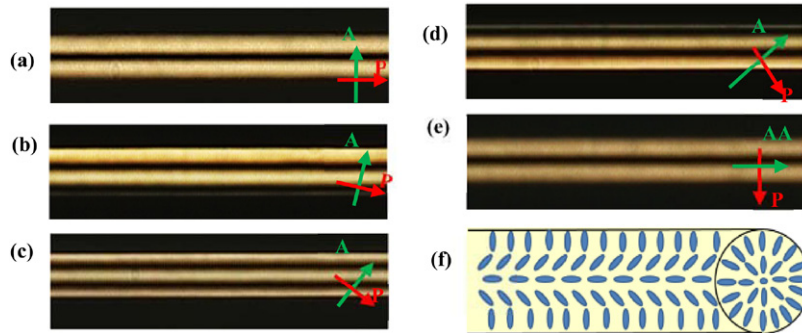


Figure 3. POM photos of the LCF observed between crossed polarizers having the angle between fiber axis and polarizer axis: (a) 0°, (b) 22.5°, (c) 45°, (d) 67.5°, and (e) 90°, respectively; and (f) schematic drawing of the LC alignment in HOF with escaped radial alignment configuration.

shows the photographs of the LCF, in which five different angles of the fiber axis to the incident linearly polarized light were set respectively. From the observed images, we confirm that the LC alignment in the air core of HOF is very uniform and well controlled by the alignment layer. Besides, the brightness of the LC-filled sample does not alter during rotation around the capillary axis. Based on these photos, we can say that the PI alignment layer indeed makes the LC directors inside the HOF axial symmetrical and orientated vertically near the capillary wall and along the capillary axis in the central area as schematically presented in figure 3(f). The non-radial LC alignment in the central area is caused by the line disclination ‘escaped’ along the axis of a cylindrical capillary [20]. This configuration is known as escaped radial or splay arrangement. Therefore, we validated that the PI layer provides the LCs inside HOF with escaped radial (or splay) configuration.

The radial alignment of NLC-infiltrated core region of the HOF as shown in figure 3(f) exhibits a mirror symmetry of two hybrid alignment NLC cells. Due to the radically axial-symmetric alignment configuration of LCs inside the micro-capillary, the optical properties of the LC fiber should be independent of the incident polarization. When a laser beam traverses the LCF at the room temperature, the experienced refractive index  $n_{LC}^{eff}$  can be approximated by the averaged extraordinary refractive index  $n_e$  and ordinary refractive index  $n_o$  of the infiltrated NLC,  $(n_e + n_o)/2$ . Indeed, this was verified by a commercial LCD simulator DIMOS 2D. It is also well known that the LC orientation and birefringence in the HOF are highly sensitive to the temperature variation [21, 22]. Thus, the effective refractive index of the LCF is considerably altered as the temperature changes.

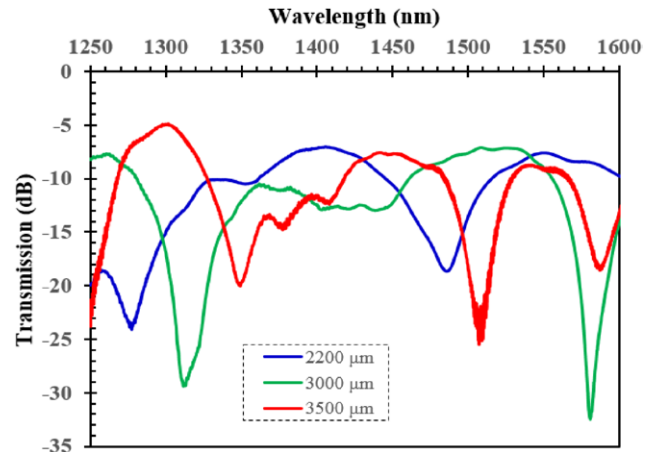
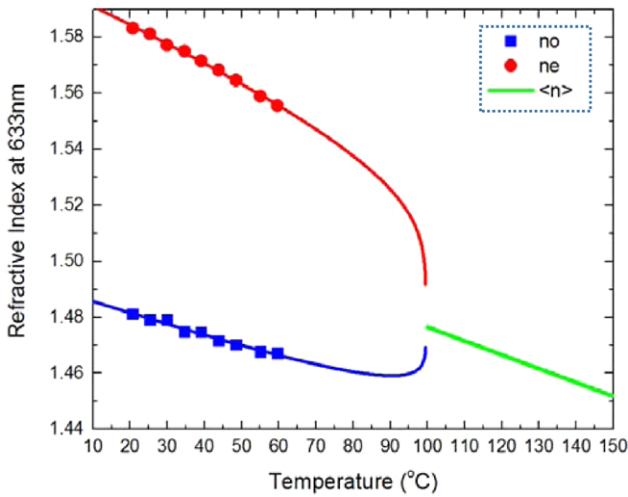
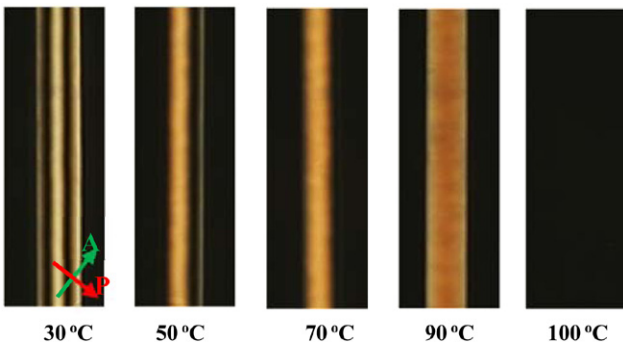


Figure 4. Measured transmission spectra of the proposed MZIs with different LCs-infiltrated lengths.

As described in the previous work [19], all fiber Mach-Zehnder interferometer (MZI) can be realized by cascading a short section of liquid crystal (LC)-filled hollow-optic fiber (HOF) between two single mode fibers. To study how the radical-aligned LCF affects the HOF-based MZI, the interference spectra of the LCF-MZIs with three LC lengths: 2.2 mm, 3.0 mm, and 3.5 mm were measured as shown in figure 4. According to the measured results, strong interferences are observed and interference fringes have a dynamic range over 25 dB. The background loss of the device is ~8 dB, which is primarily introduced by the two abrupt tapers. The average fringe spacing (FS) FS decreases with increasing the length of the LC-filled section, because the accumulated phase difference between the core and the cladding increases. Furthermore, we also find the interference properties of



**Figure 5.** Temperature-dependent refractive indices of LCT-10–1140. Blue squares and red circles are experimental data of the refractive indices  $n_o$  and  $n_e$  measured at  $\lambda = 633$  nm, as well as green line is the LC refractive index in isotropic state.



**Figure 6.** Temperature-induced birefringence variation and re-orientation of the LCs infiltrated in fiber core were observed under crossed polarizers of an optical microscope.

LCF-MZI is influenced not only by the LC length but also by the total air cavity length and tapering configuration (i.e. tapering angle and length) in this work.

For investigating the thermal-optic characterization of LCF-MZI, we measured the temperature dependent refractive indices of liquid crystal LCT-10–1140 by Abbe refractometer and the results are depicted in figure 5. The temperature of the Abbe refractometer was controlled by a circulating constant temperature bath (Atago Model 60-C3). We found the refractive indices of LCs are temperature dependent; the extraordinary refractive index ( $n_e$ ) decreases with increasing temperature, but ordinary refractive index  $n_o$  decreases first and then climbs up as the temperature approaches the clearing point, which is 99.5 °C. The crossover point for  $n_o$  is  $T_o = 89.5$  °C. Nevertheless, in the vicinity of phase transition temperature, a small temperature variation causes a dramatic change in  $\partial(n_o^{LC})/\partial T$ .

The temperature effects on the birefringence and reorientation of LCs filled in the fiber core were observed between crossed polarizers of a POM as shown in figure 6, in which the fiber axis was rotated at 45° with respect to the polarizer axis.

According to the photos, the effective index and LC orientation are considerably affected by the temperature. As the temperature increases, not only the LC’s refractive index varies, but also its tilt angle far away from the wall surface decreases gradually prone to parallel to the fiber axis with increasing temperature. This decreasing tendency of LC tilt angle with temperature agrees with the result reported by Sugiyama qualitatively [21]. Such a LC reorientation at high temperature makes the contribution of  $n_o$  dominant to the effective index of LCF. In addition, as the temperature exceeds the clear point, the LC becomes isotropic. This temperature-induced LC refractive index variation and reorientation will significantly alter the optical properties of MZI. As a result, such a fiber could be realized as a thermally tunable photonic device or temperature sensor. In our experiment, we found the LCs inside the HOF became isotropic at 100 °C, which is  $\sim 0.5$  °C higher than the clearing point measured by Differential Scanning Calorimetry (DSC, TA instrument Q100).

To study how the temperature-dependent refractive indices and LC director’s reorientation influence the spectral characteristics of the proposed MZI device, we made the LC-filled section sufficiently long to ignore the thermal expansion effect here. Under such a situation, the wavelength shift of LC-MZI fiber should be mainly contributed by the thermo-optic effect of the LCs. Besides, the silica cladding is much less sensitive to the temperature change and its temperature effect can be neglected. Consequently, the thermo-optic property of LCF-MZI can be approximated as  $\frac{\partial \lambda_m}{\partial T} \propto \frac{\partial(\delta n_{eff}^{LC})}{\partial T} \cong \frac{\partial(n_{eff}^{LC})}{\partial T}$ , where  $T$  is the temperature and  $\partial(\delta n_{eff}^{LC})/\partial T$  is the thermo-optic effect of the LC fiber material.

When the temperature increases, the heating effects give rise to changes in the effective refractive index of the LCF core and the transmission spectrum of MZI fiber. To investigate the thermal characteristics of the proposed LCF-MZI, we recorded the temperature dependent transmission spectrum from 30 °C to 130 °C (figure 7). As figure 7 shows, the measured results explicitly demonstrate the wavelength shift of the interference peak as a function of the temperature. As the temperature increases from 30 °C to 90 °C, the notch wavelength of the LCF-MZI experiences a blue shift (figures 7(a) and (b)), the progressive blue shift originates from the decreasing refractive indices of the LC. However, we found a considerable red shift (from  $\lambda = 1274$  nm to 1288.2 nm) in transmission spectrum suddenly occurs as the temperature increases from 65 °C to 70 °C (jumping from figures 7(a) and (b)). This unexpected phenomenon of the resonant wavelength jump is attribute to the change in the orders of modes interfered with each other along the propagation direction in this temperature range.

As observed in figure 6, more LC molecules tend to re-align along fiber axis (homogeneous alignment) and then  $n_o$  gradually dominates the effective refractive index with increasing temperature. This phenomenon can be verified by the results shown in figure 7(c), which indicates a red shift of the notch wavelength of MZI from 90 °C to 100 °C. This occurrence can be explained by the crossover temperature [22] of the employed LC, which is  $T_o \approx 90$  °C. Besides, in the vicinity

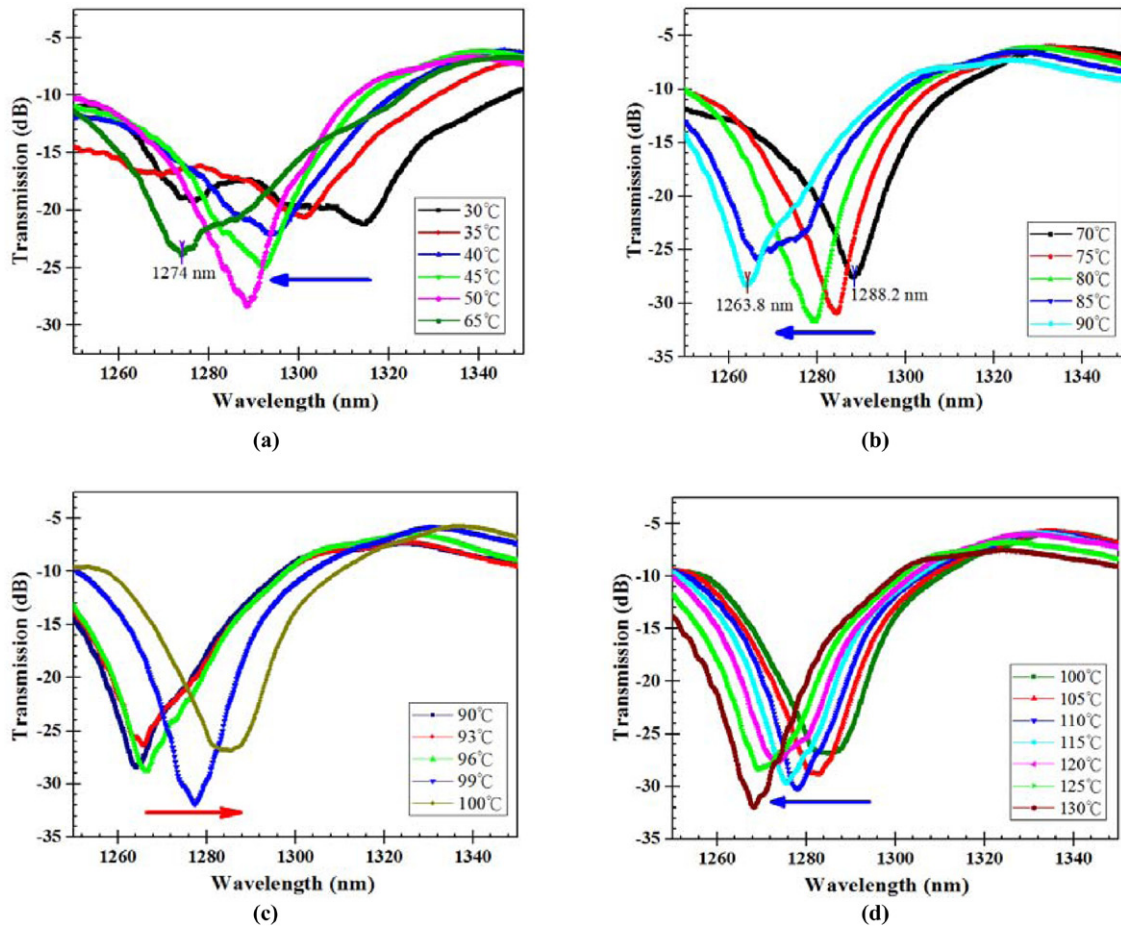


**Figure 7.** Temperature effects on the transmission spectrum of MZI under following temperature range: (a) 30 °C to 65 °C, (b) 70 °C to 90 °C, (c) 90 °C to 100 °C, and (d) 100 °C to 130 °C.

of phase transition temperature, a huge red shift of notch wavelength takes place. Such a small temperature variation causes a huge change in  $\partial(n_o^{LC})/\partial T$ , so that the sensitivity of MZI to the temperature is high. As expected, we find the tendency of wavelength shift with increasing temperature is consistent with the measured  $n_o$  temperature gradient (figure 5) at  $T_o < T < T_c$ . Moreover, as  $T > T_c$ , LC turns to an isotropic state and birefringence disappears. The refractive index decreases linearly as the temperature increases (green line in figure 5). Thus, a blue shift certainly occurs in this temperature range. Based on the data depicted in figure 7, our experimental results agree well with the prediction of the refractive index temperature gradient.

Figure 8 shows the wavelength shifts of the transmission peak of the MZI under different temperatures, in which the curve fitting process is performed. We find the curve of the temperature-induced wavelength shift can be divided into four regions. The measured wavelength shift of the MZI has a good linear behavior and the slope sensitivity is  $-2.04 \text{ nm } ^\circ\text{C}^{-1}$ ,  $0.84 \text{ nm } ^\circ\text{C}^{-1}$ ,  $4.3 \text{ nm } ^\circ\text{C}^{-1}$  and  $-0.54 \text{ nm } ^\circ\text{C}^{-1}$  in the range of 30–40 °C, 40–80 °C, 90–100 °C and 100–130 °C, respectively. Comparing the experimental results to the measured temperature-dependent refractive indices of the employed LC (figure 5), we confirm that the tunable interference peak wavelength

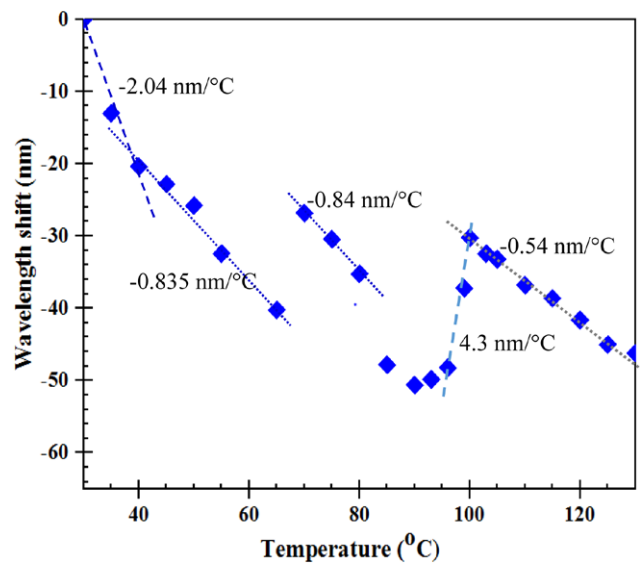


**Figure 8.** Measured transmission peak wavelength shift of the MZI fiber as a function of temperature.

mainly originates from the temperature-dependent  $n_e$  and  $n_o$  of the LC. As the temperature increases, the LC molecules far away from the core wall are significantly influenced to reorient

to the fiber axis. As a result, the contribution of  $n_o$  to the effective refractive index of LCF increases considerably. Because the temperature gradient of  $n_o$  is smaller than that of  $n_e$ , we find the tuning sensitivity  $\partial\lambda_m/\partial T$  ( $\sim 0.84 \text{ nm}/^\circ\text{C}$ ) of MZI in the medium temperature range ( $40^\circ\text{C} < T < 80^\circ\text{C}$ ) is smaller than that in the low temperature range ( $30^\circ\text{C} < T < 40^\circ\text{C}$ ). And around the crossover temperature  $T_o = 89.5^\circ\text{C}$ , the value of  $\partial\lambda_m/\partial T$  is negative when  $T < T_o$  but becomes positive when  $T > T_o$ . This positive tuning sensitivity  $\partial\lambda_m/\partial T$  auxiliary indicates the optical properties of LCF-MZI is mainly controlled by the ordinary refractive index, because more LC molecules are reoriented along the fiber axis at a high temperature. Also from figure 8, the tuning sensitivity increases dramatically as the temperature approaches  $T_c$  and then becomes linear when  $T > T_c$ , which is in good agreement with the temperature gradient of LC refractive indices.

Based on the experimental results, our LCF-based MZI has potential applications as a highly tunable photonic device or a high sensitivity temperature sensor in the temperature range of  $30\text{--}65^\circ\text{C}$ . Because the transmission dip shifts reversely for temperature on both sides of the crossover temperature and phase-transition temperature, i.e.  $89.5^\circ\text{C}$  and  $100^\circ\text{C}$ . Some different temperatures can be attributed to one specific dip at the temperature range of  $30\text{--}130^\circ\text{C}$  and make it unfavorable for wide temperature sensing range. For overcoming this problem, we can apply not only the wavelength shift, but also the minimum intensity of the spectral interference to identify the temperature. Furthermore, we successfully make use of coating a homeotropic alignment layer on the cavity-wall surface to achieve stable radical LC alignment in the hollow fiber in this work. Even though two key factors, i.e. the temperature-induced LC refractive index variation and reorientation, critically determine the output of the proposed LCF-MZI. We observe these effects on the fiber sensor performance are repeatable and stable after several experiments.

#### 4. Conclusion

We proposed and demonstrated a novel yet simple, cost-effective, compact and highly tunable fiber-optic Mach-Zehnder interferometer constructed by splicing a section of radial aligned LCF between two single mode fibers. The thermo-optical characteristics, such as temperature-induced shifts of wavelength of the spectrum, are experimentally investigated. The temperature-induced wavelength shifts of the transmission spectra of LCF-MZI are manifestly verified to be mainly contributed by the refractive indices and LC orientation inside the hollow core. The proposed interferometer utilizes two distinctive features: the core/cladding mode interference and LC which is highly sensitive to an external disturbance. Thus, the proposed LCF-MZI is highly sensitive to the temperature change and can be potentially applied as a tunable photonic device or temperature sensor. Compared to the previously reported fiber interferometer,

our LC-infiltrated MZI fiber exhibits a relatively large tunability and high sensitivity.

#### Acknowledgments

The authors are indebted to the Ministry of Science and Technology of Taiwan for financial support under contract MOST 103-2221-E-239 -003, Giantplus Tech. Corp. for providing the liquid crystal material, and technical assistance from Prof Nan-Kung Chen of the National United University, Taiwan.

#### References

- [1] Oh K, Choi S, Jung Y and Lee J W 2005 Novel hollow optical fibers and their applications in photonic devices for optical communications *J. Lightwave Technol.* **23** 524–32
- [2] Choi S, Eom T J, Yu J W, Lee B H and Oh K 2002 Novel all-fiber bandpass filter based on hollow optical fiber *IEEE Photon. Technol. Lett.* **14** 1701–3
- [3] Shin W, Oh K, Yu B-A, Lee Y L, Noh Y-C, Ko D-K and Lee J 2008 All-fiber wavelength-tunable and mode convertible bandpass filter for optical interconnections *IEEE Photon. Technol. Lett.* **20** 404–6
- [4] Choi S, Oh K, Shin W, Park C S, Paek U C, Park K J, Chung Y C, Kim G Y and Lee Y G 2002 Novel mode converter based on hollow optical fiber for gigabit LAN communication *IEEE Photon. Technol. Lett.* **14** 248–50
- [5] Choi S, Eom T J, Jung Y, Lee B H, Lee J W and Oh K 2005 Broad-band tunable all-fiber bandpass filter based on hollow optical fiber and long-period grating pair *IEEE Photon. Technol. Lett.* **17** 115–7
- [6] St P, Russell J, Hölzer P, Chang W, Abdolvand A and Travers J C 2014 Hollow-core photonic crystal fibres for gas-based nonlinear optics *Nat. Photon.* **8** 278–86
- [7] Choi S Y, Cho D K, Song Y-W, Oh K, Kim K, Rotermund F and Yeom D-I 2012 Graphene-filled hollow optical fiber saturable absorber for efficient soliton fiber laser mode-locking *Opt. Exp.* **20** 5652–7
- [8] Jiang M-S, Sui Q-M, Jin Z-W, Zhang F-Y and Jia L 2014 Temperature-independent optical fiber Fabry–Perot refractive-index sensor based on hollow-core photonic crystal fiber *Optik* **125** 3295–8
- [9] Jung H, Seo Y G, Ha W, Kim D-K, Park S H and Oh K 2009 Mask-free hybrid long-period fiber grating fabrication by self-assembled periodic polymerization in silica hollow optical fiber *Opt. Lett.* **34** 2745–7
- [10] Rutkowska K A, Milenko K, Chojnowska O, Dąbrowski R and Woliński T R 2015 Light propagation mechanism switching in a liquid crystal infiltrated microstructured polymer optical fibre *Opto-Electron. Rev.* **23** 252–8
- [11] Cai D-P, Nien S-C, Chiu H-K, Chen C-C and Lee C-C 2011 Electrically tunable liquid crystal waveguide attenuators *Opt. Express* **19** 11890–6
- [12] Oh Y, Kwon M and Shin S 2004 In-line polarization controller that uses a hollow optical fiber filled with a liquid crystal *Opt. Lett.* **29** 2605–7
- [13] Ptilakis A K, Zografopoulos D C and Kriezis E E 2011 In-line polarization controller based on liquid-crystal photonic crystal fibers *J. Lightwave Technol.* **29** 2560–9
- [14] Du F, Lu Y Q and Wu S T 2004 Electrically tunable liquid-crystal photonic crystal fiber *Appl. Phys. Lett.* **85** 2181–3

- [15] Hsu C-H, Choi W-K and Wang L A 2015 A novel fabrication of fiber Bragg grating in hollow-core fiber with HPDLCs *Proc. SPIE 9449, The Int. Conf. on Photonics and Optical Engineering (icPOE 2014)*, 94491T-1 p 5
- [16] Zito G and Pissadakis S 2013 Holographic polymer-dispersed liquid crystal Bragg grating integrated inside a solid core photonic crystal fiber *Opt. Lett.* **38** 3253–6
- [17] Zhang S, Zhang W, Geng P and Wang L 2014 A Mach–Zehnder interferometer constructed using lateral offset and a long period fiber grating for two-dimensional bending vector sensing *J. Opt.* **16** 015501
- [18] Yang J, Jiang L, Wang S, Li B, Wang M, Xiao H, Lu Y and Tsai H 2011 High sensitivity of taper-based Mach–Zehnder interferometer embedded in a thinned optical fiber for refractive index sensing *Appl. Opt.* **50** 5503–7
- [19] Ho B-Y, Su H-P, Tseng Y-P, Wu S-T and Hwang S-J 2015 Temperature effects of Mach–Zehnder Interferometer using a liquid crystal-filled fiber *Opt. Express* **23** 33588–96
- [20] Chychłowski M, Yaroshchuk O, Kravchuk R and Woliński T 2012 Liquid crystal alignment in cylindrical microcapillaries *Opto-Electron. Rev.* **20** 8–13
- [21] Sugiyama T, Kuniyasu S and Kobayashi S 1993 Temperature dependence of pretilt angle in nematic liquid crystal cell *Mol. Cryst. Liq. Cryst.* **23** 199–214
- [22] Li J, Gauzia S and Wu S-T 2004 High temperature-gradient refractive index liquid crystals *Opt. Express* **12** 2002–10